Available online at www.sciencedirect.com
SCIENCE DIRECT
Materials Research Bulletin 40 (2005) 2189–2197
Materials Research Bulletin
www.elsevier.com/locate/matresbu

Spectroscopic properties of Yb^{3+} in heavy metal contained fluorophosphate glasses

J.H. Choi [a], A. Margaryan [b], Ashot Margaryan [b], F.G. Shi [a,*]

[a] *Optoelectronic Materials and Packaging Lab., Department of Chemical Engineering and Material Science, University of California, Irvine, CA 92697, USA*
[b] *AFO Research Inc., Glendale, P.O. Box 1934, CA 91209, USA*

Received 8 September 2004; received in revised form 2 April 2005; accepted 30 June 2005
Available online 8 August 2005

Abstract

A new series of $20Bi(PO_3)_3$–$10Sr(PO_3)_2$–$35BaF_2$–$35MgF_2$ doped with Yb^{3+} is introduced for fiber and waveguide laser applications. The stimulated emission cross-section σ_{emi}, which was found to be 1.37 pm^2 at the lasing wavelength of 996 nm, is the highest one among fluorophosphate glasses. It has been found that an extremely high gain coefficient of $G = 1.65$ ms pm^4 and high quantum efficiency of $\eta = 93\%$ for 1 wt.% Yb_2O_3 doped systems. The various concentration effects on laser performance properties including minimum pumping intensity I_{min}, the minimum fraction of excited ions β_{min} and the saturation pumping intensity I_{sat} are analyzed as a function of Yb_2O_3 concentration. Those results obtained in current system had advantage over some fluorophosphate glasses reported.

Keywords: A. Glasses; D. Luminescence

1. Introduction

Yb-doped laser glasses have many attractive properties because of the small quantum defect three times less than Nd^{3+} on the 1.06 μm transition and the broad band fluorescence spectrum compared with Nd^{3+} which provides sufficient bandwidth to generate and amplify ultrashort laser pulses [1,2]. In addition, Yb^{3+} doped laser glasses are attractive for high power lasers to be needed for next-generation

* Corresponding author.
E-mail address: fgshi@uci.edu (F.G. Shi).

0025-5408/$ – see front matter © 2005 Elsevier Ltd. All rights reserved.
doi:10.1016/j.materresbull.2005.06.015

nuclear fusion and as a sensitizer of energy transfer for infrared to visible up-conversion and infrared laser [3]. Therefore, host material for solid-state laser led to the development of various Yb-doped glass bulk laser or fiber form for lasers and amplifiers.

Among potential active dopant host materials, fluorophosphate glasses are promising because of its potential for hosting various rare earth dopants [4–8]. Fluorophosphates glasses can also offer improved optical properties, such as low non-linear refractive index, low phonon energy and high transparency from near UV to mid-IR [9–11]. For fiber lasers, it is desirable for the emission cross-section to be as large as possible in order to achieve a high gain for a short length of fiber and for compact planar waveguide lasers or microchip lasers. Unfortunately, the reported fluorophosphate glasses have a low emission cross-section, i.e., $<0.5 \times 10^{-21}$ cm^2, which is not sufficient for the diode-pumped short pulse laser applications [12–15]. In previous works including Nd^{3+} and Er^{3+} doped systems, it has shown that Yb-doped fluorophosphate glass with high stimulate emission cross-section of 0.87 pm^2 and extremely high gain coefficient of 0.95 ms pm^4 exhibits an excellent candidate material for fiber and waveguide lasers [16–18]. In order to improve spectroscopic and lasing performance compared to previously developed fluorophosphates glasses for fiber and waveguide lasers, the fluorophosphate glass are incorporated by bismuth metaphosphate because the stimulated emission cross-section of rare earth ions increases with the refractive indices of the hosts which might provide a broadband amplication [19,20].

In this paper, the spectroscopic properties of Yb^{3+} activated bismuth contained fluorophosphates laser glasses were investigated. The emission cross-section, absorption cross-section, gain coefficient, quantum efficiency and the minimum pumping intensity were investigated in order to assess their capabilities of being used as fiber and waveguide lasers. And then spectroscopic and laser performance properties were compared with some laser host glasses reported and fluorophosphate glass previously developed.

2. Experiment procedures and data analysis

2.1. Glass synthesis

Starting materials are from MgF_2, BaF_2, $Bi(PO_3)_3$ and $Sr(PO_3)_2$ (City Chemicals) and Yb_2O_3 (Spectrum Materials) with 99.99%. A series of starting materials were weighed according to $20Bi(PO_3)_3$–$10Sr(PO_3)_2$–$35BaF_2$–$35MgF_2$ and mixed thoroughly. The raw materials were melted in a vitreous carbon crucible in Ar-atmosphere at 1150–1200 °C for 1 h. The quenched samples were annealed at 400 °C to remove internal stress. The residual stress was examined by the polariscope (Rudolph Instruments). Samples were cut and polished by the size of 15 mm × 10 mm × 2 mm for optical and spectroscopic measurements.

2.2. Spectroscopic property measurement

The refractive index was measured with a unit of Abbe refractometer (ATAGO) at 20 °C. The absorption spectra were measured by Perkin-Elmer (Lambda 900) spectrometer in the range of 800–1200 nm at room temperature. The emission spectra were obtained by the 950 nm excitation of Ti:sapphire laser pumped by an Ar ion laser and dispersed onto a monochrometeor (Oriel) and detected

with Si pin detector (Thorlab). The spectra were amplified with a lock in amplifier (Amteck 5150). The lifetime of the excited state was determined with a Q-switched Nd:YAG laser pumped by an OPO (Continuum Surelite). The duration of the pulses was 5 ns. The fluorescent radiation is detected using a Si pin photodiode (Thorlabs) via an interference filter (Edmund Scientific). The signal was collected on a fast oscilloscope (LeCroy 9350:500 MHz) and transferred to a computer for data analysis.

2.3. Data analysis

From the absorption spectra, the spontaneous transition probability A_{rad} is experimentally determined by using following relationship [21],

$$A_{rad} = \frac{8\pi cn(\lambda_p)^2(2J'+1)}{\lambda_p^4(2J+1)} \int k(\lambda)\,d\lambda \tag{1}$$

where J' and J are the total momentum for the upper and lower levels, respectively. λ_p is the absorption peak wavelength, and $\int k(\lambda)\,d\lambda$ is integrated absorption cross-section which is integrated with respect to absorption cross-section $\sigma_{abs}(\lambda)$. $n(\lambda_p)$ is the refractive index at each absorption peak wavelength which was determined by using Cauchy's equation, $n(\lambda) = A + B/\lambda^2$. The absorption cross-section can be obtained by using Eq. (2) [22], i.e.

$$\sigma_{abs} = \frac{2.303\log(I_o/I)}{NL} \tag{2}$$

where N is Yb^{3+} ion concentration (ion/cm^3) and L is the thickness of the sample. There are two most usual methods to determine the emission cross-section σ_{emi} for the $^2F_5$–$^2F_{7/2}$ transition of Yb^{3+}. The one to obtain the emission cross-section σ_{emi} using integrated absorption cross-section $\int k(\lambda)\,d\lambda$ was given by the Fuchtbauer–Landenburg Eq. (3) [22], i.e.

$$\sigma_{emi} = \frac{\lambda_p^4 A_{rad}}{8\pi cn(\lambda_p)^2 \Delta\lambda_{eff}} = \frac{4\int k(\lambda)\,d\lambda}{3\Delta\lambda_{eff}} \tag{3}$$

where λ_p is the wavelength of the absorption peak, c the speed of light in vacuum, $n(\lambda_p)$ the refractive index at emission peak wavelength and $\Delta\lambda_{eff}$ is the effective fluorescence linewidth. The latter is the reciprocity method based on McCumber Eq. (4) [21,23],

$$\sigma_{emi}(\lambda) = \sigma_{abs}(\lambda)\frac{Z_l}{Z_u}\exp\left(\frac{E_{Zl} - hc\lambda^{-1}}{kT}\right) \tag{4}$$

where Z_l, Z_u and k are the partition functions of the lower, upper levels and the Boltzmann's constant, respectively. The reciprocity method may be employed for host materials with appropriate energy level data. The zero line energy E_{Zl}, which is defined to be the energy separation between the lowest components of the upper and lower field states, is associated with the strongest peak in absorption spectra of Yb^{3+}. In the high temperature limit, the ratio of Z_l/Z_u becomes the degeneracy weighting of the two states corresponding to the $^2F_{7/2}$–$^2F_{5/2}$ transition [21]. Since the ratio of Z_l/Z_u does not change distinctively with respect to various glass materials, thus the value of Z_l/Z_u has been 4/3 at room temperature [24].

In order to assess the potential of the real Yb^{3+} doped glass as a laser material, several important parameters such as the minimum pumping intensity I_{min}, the minimum fraction of excited ions β_{min} and the saturation pumping intensity I_{sat} should be determined. The minimum absorbed pumping intensity I_{min}, which is required for the transparency to be achieved at the lasing wavelength λ_0, is calculated by the following Eqs. (5) and (6) [25],

$$I_{min} = \beta_{min} \times I_{sat} \tag{5}$$

and β_{min} is given by

$$\beta_{min} = \frac{\sigma_{abs}(\lambda_0)}{\sigma_{emi}(\lambda_0) + \sigma_{abs}(\lambda_0)} = \left\{1 + \frac{Z_l}{Z_u}\exp\left[\frac{(E_{Zl} - hc\lambda_0^{-1})}{kT}\right]\right\}^{-1} \tag{6}$$

In Eq. (6), $\sigma_{abs}(\lambda_0)$ and $\sigma_{emi}(\lambda_0)$ represent the absorption and the emission cross-section at the lasing wavelength λ_0.

$$I_{sat} = \frac{hc}{\lambda_p \tau_l \sigma_{abs}(\lambda_p)} \tag{7}$$

where λ_p and τ_f represent the excitation wavelength and the fluorescence lifetimes after fitting the measured values to the first order exponentials, and $\sigma_{abs}(\lambda_p)$ is the absorption cross-section at the absorption wavelength.

The gain coefficient G ($\sigma_{abs}(\lambda_p) \times \tau_f \times \sigma_{emi}$) is closely related to the product of absorption cross-section $\sigma_{abs}(\lambda_p)$, emission cross-section σ_{emi} and fluorescence lifetime τ_f as below [26]

$$G = N \propto E_p \propto \sigma_{abs}(\lambda_p) \propto \tau_l \propto \sigma_{emi} \propto \sigma_{abs}(\lambda_p) \times \sigma_{emi} \propto \tau_f \tag{8}$$

where N, E_p are the rare earth dopant concentration and pump energy independent of host, respectively. Therefore, the gain coefficient G is proportional to $\sigma_{abs}(\lambda_p) \times \sigma_{emi} \times \tau_f$. The product of absorption cross-section $\sigma_{abs}(\lambda_p)$ and fluorescence lifetime τ_f is proportion to the stored energy and the one of emission cross-section σ_{emi} and fluorescence lifetime τ_f is proportion to extraction efficiency. The higher stored energy and extraction efficiency gives better potentials for laser host materials. It, therefore, has been suggested that the laser glass should have high gain coefficient G for laser applications.

3. Results and discussion

3.1. Dependence of spectroscopic properties on Yb_2O_3 concentration

Fig. 1 shows the emission and absorption spectra of Yb^{3+} in fluorophosphate glass doped with 1.5 wt. Yb_2O_3. The center peak of absorption of the $^2F_{7/2}$–$^2F_{5/2}$ transition, which corresponds to the energy separation of the lowest crystal field components of the ground and excited state, is located at 977 nm and the peaks of emission bands are located at 997 nm. Table 1 lists some of the spectroscopic properties; the absorption cross-section $\sigma_{abs}(\lambda_p)$, the emission cross-section, the spontaneous transition probability A_{rad}, radiative lifetime τ_{rad}, and figure of merits $\tau_f \times \sigma_{emi}$. As shown in Table 1, the absorption cross-section $\sigma_{abs}(\lambda_p)$ at zero line absorption peak and spontaneous transition probability A_{rad} of to the $^2F_{7/2}$–$^2F_{5/2}$ transition exhibit a maximum at 1 wt. Yb_2O_3 and then shorten with an increase in Yb_2O_3 concentration.

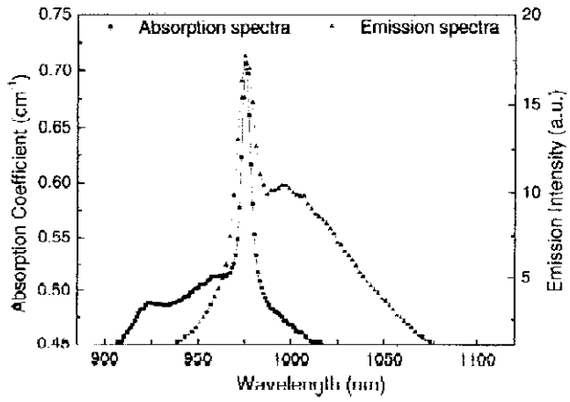

Fig. 1. Absorption and emission spectra of Yb^{3+} in the new fluorophosphate glass doped with 1.5 wt. Yb_2O_3.

In addition, the fluorescence lifetime τ_f of Yb^{3+} from upper laser level linearly shortens from 0.66 to 0.41 ms, which indicates that the quenching effect of lifetime τ_f of Yb^{3+} exists with an increase in Yb_2O_3 concentration. But the radiative lifetime determined by the spontaneous transition probability A_{rad} increases from 0.71 to 1.2 ms as Yb_2O_3 concentration increase up to 3 wt.

3.2. *The relationship between the integrated absorption cross-section* $\int \sigma_{abs}\, d\lambda$ *and emission cross-section* σ_{emi}

The relationship between the integrated absorption cross-section $\int \sigma_{abs}\, d\lambda$ and emission cross-section σ_{emi} for Yb^{3+} doped fluorophosphates glasses is shown in Fig. 2. As shown in Eq. (5) above, the emission cross-section σ_{emi} is closely related to the integrated absorption cross-section $\int \sigma_{abs}\, d\lambda$. Linearity between them is observed in Fig. 2, which indicates that the emission cross-section σ_{emi} strongly depends on integrated absorption cross-section $\int \sigma_{abs}\, d\lambda$. Emission cross-section σ_{emi} obtained through Fuchtbauer–Ladernburg method is to be assessed again for the reasonableness by using reciprocity method i.e. (4). The discrepancies between two values of emission cross-section are found to be below 10%, which shows that both methods are effective and appropriate for the determination of emission cross-section σ_{emi}.

Table 1
Variation of spectroscopic properties of Yb^{3+} doped bismuth contained fluorophosphate glasses as a function of Yb_2O_3 concentration

Yb_2O_3 (wt.)	Refractive index (n_D)	$\sigma_{abs}(\lambda_p)$ (pm^2)	A_{rad} (s^{-1})	τ_{rad} (ms)	σ_{emi} (λ_0) (pm^2)	τ_f (ms)	$\tau_f \times \sigma_{emi}$ (ms pm^2)
1	1.6532	1.77	1406	0.71	1.39	0.66	0.93
1.5	1.6539	1.24	1149	0.87	1.25	0.59	0.75
2	1.6542	1.46	953	1.05	0.97	0.5	0.49
3	1.6549	1.39	832	1.20	0.72	0.41	0.29

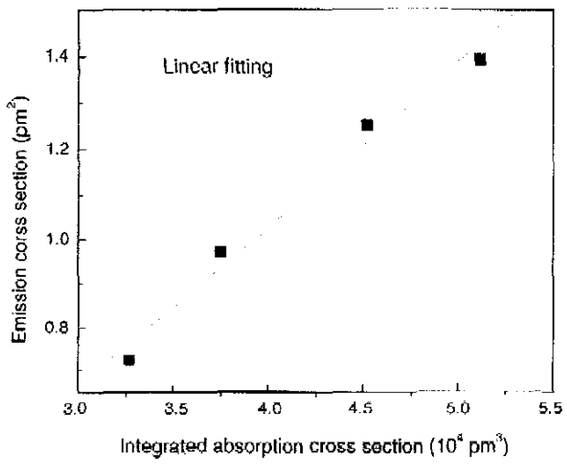

Fig. 2. Relationship between the integrated absorption cross-section $\left(\int \sigma_{abs}\, d\lambda\right)$ and the emission cross-section (σ_{emi}).

3.3. The variation of the integrated absorption cross-section $\int \sigma_{abs}\, d\lambda$ and effective linewidth $\Delta\lambda_{eff}$

Fig. 3 shows the variation of the integrated absorption cross-section $\int \sigma_{abs}\, d\lambda$ and effective linewidth $\Delta\lambda_{eff}$ as a function of Yb_2O_3 concentration. The emission cross-section σ_{emi}, which is determined by the Fuchtbauer–Ladernburg method at 996 nm, monotonically decreases with an increase in Yb_2O_3 concentration. Based on the Fuchtbauer–Ladernburg method, the emission cross-section σ_{emi} is determined by the integrated absorption cross-section $\int \sigma_{abs}\, d\lambda$ and effective linewidth $\Delta\lambda_{eff}$. According to relationship between the integrated absorption cross-section $\int \sigma_{abs}\, d\lambda$ and emission cross-section σ_{emi} in Fig. 2, it is evident that the increase of integrated absorption cross-section $\int \sigma_{abs}(\lambda_p)$ gives rise to an increase in the emission cross-section σ_{emi} as shown in Fig. 3. On the other hand, the linear increase in the

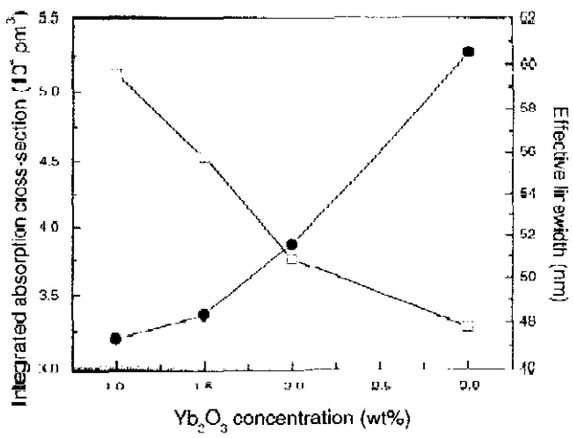

Fig. 3. Integrated absorption cross-section $\left(\int \sigma_{abs}\, d\lambda\right)$ and effective linewidth ($\Delta\lambda_{eff}$) as a function of Yb_2O_3 concentration; Lines are drawn as a guide for eyes.

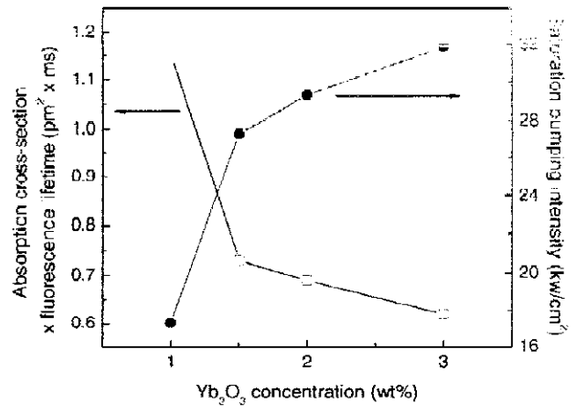

Fig. 4. Relationship between the product of the absorption cross-section and fluorescence lifetime ($\sigma_{abs}(\lambda_p) \times \tau_f$) and saturation pumping intensity (I_{sat}) as a function of Yb_2O_3 concentration: Lines are drawn as a guide for eyes.

effective linewidth $\Delta\lambda_{eff}$ leads to a decrease in the emission cross-section σ_{emi} as Yb^{3+} concentration increases. Consequently, the counterbalance of two effects between integrated absorption cross-section $\int \sigma_{abs}\, d\lambda$ and the effective linewidth $\Delta\lambda_{eff}$ leads emission cross-section σ_{emi} to slightly decrease with an increase in Yb_2O_3 concentration.

3.4. Concentration effects on laser performance properties

The various concentration effects on laser performance properties including minimum pumping intensity I_{min}, the minimum fraction of excited ions β_{min} and the saturation pumping intensity I_{sat} are explained as Yb_2O_3 concentration increases. Fig. 4 shows the relationship of the product of absorption cross-section and fluorescence lifetime $\sigma_{abs}(\lambda_p) \times \tau_f$ and saturation pumping intensity I_{sat} $\sigma_{abs}(\lambda_p) \times \tau_f$ almost exponentially decreases from 1.17 to 0.57 ms pm^2 and saturation pumping intensity I_{sat} increases from 17.06 to 34.98 kW/cm^2 with an increase in Yb_2O_3 concentration. When $\sigma_{abs}(\lambda_p) \times \tau_f$ becomes lower, the saturation pumping intensity I_{sat} increases with an increase in Yb_2O_3 concentration, which is consistent with Eq. (7). In other world, it is desirable for the saturation pumping intensity I_{sat} to be as low as possible to minimize the minimum pumping intensity I_{min} since the emission cross-section $\sigma_{emi}(\lambda)$ is proportional to $\sigma_{abs}(\lambda_p)$ as shown in Eq. (4). Incidentally, the minimum fraction of excited ions (β_{min})

Table 2
Variation of laser performance properties of Yb^{3+} doped bismuth contained fluorophosphate glasses as a function of Yb_2O_3 concentration

Yb_2O_3 (wt.%)	β_{min}	I_{sat} (kW/cm^2)	I_{min} (kW/cm^2)	G (ms pm^4)
1	0.21	17.3	3.7	1.65
1.5	0.21	29	5.8	0.94
2	0.21	27	6.0	0.72
3	0.21	31	6.9	0.42

Table 3
Comparisons of spectroscopic properties with some fluorophosphate glasses with high fluorine

Host glasses	n_d	λ_{zl} (nm)	σ_{abs} (λ_0) (pm^2)	σ_{emi} (λ_0) (pm^2)	τ_f (ms)	$\tau_f \times \sigma_{emi}$ (ms pm^4)	References
FP[a]	≅1.5	1020	0.43 (p)	0.5	1.2	0.6	[14]
FP	≅1.5	970	0.4	0.2	1.3	0.26	[15]
FP15	1.472	1001	–	0.49	1.6	0.78	[27]
MBBA	1.5476	976	0.29	0.87	0.65	0.57	[14]
Fluorophosphate	1.6229	977	0.31	1.39	0.66	0.93	Current work

does not change very much with increasing Yb_2O_3 concentration. It is thus apparent for minimum pumping intensity I_{min} closely to be proportion to saturation pumping intensity I_{sat} following Eq. (7).

Table 2 shows the variation of the minimum pump intensity I_{min} and gain coefficient G as a function of Yb_2O_3 concentration. Gain coefficient G, i.e. the stored energy and extraction efficiency, falls from 1.65 to 0.42 ms pm^4 and minimum pump intensity I_{min}, which shows the ease of pumping the material to achieve laser action, dramatically rise from 3.7 to 6.9 kW/cm^2 with an increase in Yb_2O_3 concentration. The gain coefficient G is entirely used to evaluate the laser performance in terms of stored energy and extraction efficiency. It is apparent that the decrease of the gain coefficient G results from the decrease of the absorption cross-section $\sigma_{abs}(\lambda_p)$, emission cross-section σ_{emi} and the fluorescence lifetime τ_f with an increase in Yb_2O_3 concentration. In this glass system, the concentration quenching of Yb^{3+} is observed but the value of gain coefficient G is still much higher than ever among fluorophosphates glass even at high concentration of Yb^{3+} [14]. The overall comparisons on spectroscopic and laser performance properties in fluorophosphate glasses with high fluorine are listed in Table 3. The incorporation of bismuth phosphate leads to increase absorption cross-section, emission cross-section and figure of merit in the same concentration of Yb_2O_3.

4. Conclusions

A new series of $20Bi(PO_3)_3$–$10Sr(PO_3)_2$–$35BaF_2$–$35MgF_2$ glasses doped with Yb^{3+} has successfully been developed. A systematic investigation of spectroscopic properties from the absorption and emission spectra has been performed as a function of Yb_2O_3 concentration. The best laser performance is found in the fluorophosphate glass doped with 1 wt. Yb_2O_3. The emission cross-section σ_{emi}, which was found to be 1.37 pm^2 at the lasing wavelength of 997 nm, is the highest one among fluorophosphate glasses to our knowledge. It has been found that an extremely high gain coefficient of $G = 1.65$ ms pm^4 and high quantum efficiency of $\eta = 93\%$. Those results obtained in current system had advantage over some fluorophosphate glasses reported, which implies that the current Yb^{3+} activated $20Bi(PO_3)_3$–$10Sr(PO_3)_2$–$35BaF_2$–$35MgF_2$ glass is an excellent candidate material for fiber and waveguide lasers.

References

[1] T.Y. Pan, IEEE J Quantum Electron. QE-29 (1993) 1457.
[2] G. Wang, S. Xu, S. Dai, J. Zhang, Z. Jiang, J. Alloys Compd. 373 (2004) 246.
[3] B. Peng, T. Izumitani, Rev. Laser Eng. 21 (1993) 1234.

[4] J.F. Philips, T. Topfer, H. Ebendorff-Heidepriem, D. Ehrt, R. Sauerbrey, Appl. Phys. B 72 (2001) 399.
[5] O. Deutschbein, M. Faultisch, W. Jahn, G. Krolla, N. Neuroth, Appl. Opt, 17 (1978) 2228.
[6] J.H. Choi, F.G. Shi, A. Margaryan, A. Margaryan, W.E. van der Veer, Proc. SPIE 4974 (2003) 106.
[7] J.H. Choi, F.G. Shi, A. Margaryan, A. Margaryan, Proc. SPIE 4974 (2003) 121.
[8] A. Margaryan, J.H. Choi, A. Margaryan, F.G. Shi, Appl. Phys. B 78 (2004) 409.
[9] S.V.J. Lkshmn, Y.C. Ratnkaran, Phys. Chem. Glasses 29 (1988) 26.
[10] B. Viana, M. Palazzi, O. LeFol, J. Non-Cryst. Solids 215 (1997) 96.
[11] S. Jiang, T. Luo, B.C. Hwang, F. Smekatala, K. Seneschal, J. Lucas, N. Peyghambarian, J. Non-Cryst. Solids 263–264 (2000) 364.
[12] M. Weber, J.E. Lynch, D.H. Blachburn, D.J. Cronin, IEEE J. Quantum Electron QE-19 (1983) 1600.
[13] V. Petrove, U. Griebner, D. Hert, W. Seeber, Opt. Lett. 22 (1997) 365.
[14] C. Hönninger, R. Paschotta, M. Graf, M. Graf, F. Morier-Genoud, G. Zhang, M. Moser, S. Biswal, J. Nees, A. Braun, G.A. Mourou, I. Johannsen, A. Giesen, W. Seeber, U. Keller, Appl. Phys. B 69 (1999) 3.
[15] I. Yasui, H. hagihara, H. Inoue, J. Non-Cryst. Solids 140 (1992) 130.
[16] J.H. Choi, A. Margaryan, A. Margaryan, F.G. Shi, J. Mater. Res. 20 (2005) 264.
[17] J.H. Choi, A. Margaryan, A. Margaryan, F.G. Shi, J. Alloys Compd. 396 (2005) 79.
[18] J.H. Choi, A. Margaryan, A. Margaryan, F.G. Shi, J. Lum. 114 (2005) 167.
[19] R. Reisfeld, Struct. Bonding 22 (1975) 123.
[20] Y. Ohishi, A. Mori, M. Yamada, H. Ono, Y. Nishida, K. Oikawa, Opt. Lett. 23 (1998) 274.
[21] X. Zou, H. Toratani, Phys. Rev. B 52 (22) (1995) 15889.
[22] S.A. Payne, L.L. Chase, L.K. Smith, et al. IEEE J. Quantum Electron. 28 (1992) 2619.
[23] H. Takebe, T. murata, K. Morinaga, J. Am. Ceram. Soc. 79 (1996) 681.
[24] L. Zhang, H. Hu, J. of Non-Cryst. Solids 292 (2001) 108.
[25] L.D. Deloach, S.A. Payne, L. Smith, W.L. kway, W.F. Krupke, J. Opt. Soc. Am. B11 (1994) 269.
[26] J. Chun, Z. Junzhou, D. Peizhen, H. Cuosong, M. Hanfen, F. Gan, Sci. Chin. 42 (1999) 616.
[27] H. Yin, P. Deng, J. Zhang, F. Gan, J. Non-Cryst. Solids 210 (1997) 248.